# We are IntechOpen, the world's leading publisher of Open Access books Built by scientists, for scientists

**4,800**
Open access books available

**122,000**
International authors and editors

**135M**
Downloads

Our authors are among the

**154**
Countries delivered to

**TOP 1%**
most cited scientists

**12.2%**
Contributors from top 500 universities

CLARIVATE ANALYTICS BOOK CITATION INDEX INDEXED

WEB OF SCIENCE™

Selection of our books indexed in the Book Citation Index in Web of Science™ Core Collection (BKCI)

## Interested in publishing with us?
## Contact book.department@intechopen.com

Numbers displayed above are based on latest data collected.
For more information visit www.intechopen.com

10

# Dimensionless Parametric Analysis of Spark Ignited Free-Piston Linear Alternator

Jinlong Mao, Zhengxing Zuo and Huihua Feng
*School of Mechanical Engineering,*
*Beijing Institute of Technology, Beijing,*
*China*

## 1. Introduction

The decreasing crude oil sources, the increasing concern about greenhouse gas pollution, and the strict emission standards force researchers into never-ending effort to design less polluting and more fuel efficient vehicles. Free-piston linear alternator (FPLA) which is a free-piston engine coupled to a linear alternator, converting piston's kinetic energy into electricity directly, has attracted considerable research interests recently by a number of research groups worldwide due to its potential advantages listed bellow:

1. High efficiency. 1) Direct conversion of piston motion into electric energy with shorter energy transferring path. 2) Reduction of friction between piston ring and cylinder wall due to the elimination of the dynamic piston side forces.
2. High power capacity. With a free-piston engine, heavy mechanical components as crankshaft, flywheel and camshaft are eliminated and the generator is integrated into the engine directly. Therefore, the power-train will have fewer components, lower weight and also occupies less space.
3. Controllable compression ratio. The stroke and thus the compression ratio can be dynamically controlled through the electrical load.
4. Multi-fuel feasibility. The variable compression ratio feature provides the opportunity for the engine to be operated with wide range of fuels [1].
5. Few moving parts. There is only one major moving part: the piston, connecting rod and translator assembly. As a consequence, the engine requires less lubrication and has less friction wear.
6. Good transient response. The free-piston engine reaches its operating point almost immediately since it does not have any energy accumulators, such as flywheel [2].

In the recent two decades, some literatures have already been published about the design and numerical simulation of FPLA. Martin Goertz and Lixin Peng evaluated several feasible hybrid power-train concepts and the results indicated that free-piston linear generator was one of the most promising candidates of the future power-train configuration [3]. West Virginia University had already demonstrated stable operation of a spark ignited FPLA prototype with bore of 36.5mm, maximum possible stroke of 50mm and 316W output power was produced at 79V working at full load [4]. Ehab Shoukry did some research about parametric study of a two-stroke direct injection linear engine using zero dimensional single zone models [5].The European Union has been doing a subject of

Free-piston Energy Converter (FPEC) since 2002 aimed to develop an efficient new technology suitable for vehicle propulsion, auxiliary power unit and distributed power generation. The design and optimization of linear alternator and crankless engine, control strategy, numerical simulation and power management have been carried out systemically [6]. Dr. Peter Van Blarigan at Sandia National Laboratory presented the design of a dual piston free-piston engine generator with 40kW electric power output and the engine employed homogeneous charge compression ignition (HCCI) operating on a variety of hydrogen-containing fuels [7, 8]. Jakob Fredriksson and Ingemar Denbratt at Chalmers University of Technology investigated a two-stroke free-piston engine with different fuels using BOOST and SENKIN [9]. Czech Technical University had successfully developed a direct injection FPLA prototype recently, and steady operation had been realized based on precise motion control. When the prototype was running with frequency of 27Hz and compression of 9, the average power output was approximately 350W, but the efficiency had not been reported [10]. Mikalsen and Roskilly proposed a design of a single cylinder free-piston engine generator with gas-filled bounce chamber, simulated its working process and discussed the effects of parameters in a wide operating range to the engine's performance [11]. A novel approach of modeling the free-piston engines through the introduction of solution-dependent mesh motion in an engine CFD toolkit OpenFOAM was also presented [12].

Dimensionless analysis using Buckingham's π theory was performed base on the parameters of a spark ignited FPLA prototype (as can be seen in Fig.1) in the following contents. The objectives of this work are:

- To decrease the number of variables and still use the equations involved in the modeling of FPLA.
- To generalize the study of FPLA to a wide range of geometrical designs in order to find out the best geometric dimensions with most favorable performance.
- To establish a scale for the similitude concept so the experiments done on the existing prototype could be used to predict performances for FPLA with various sizes and dimensions.

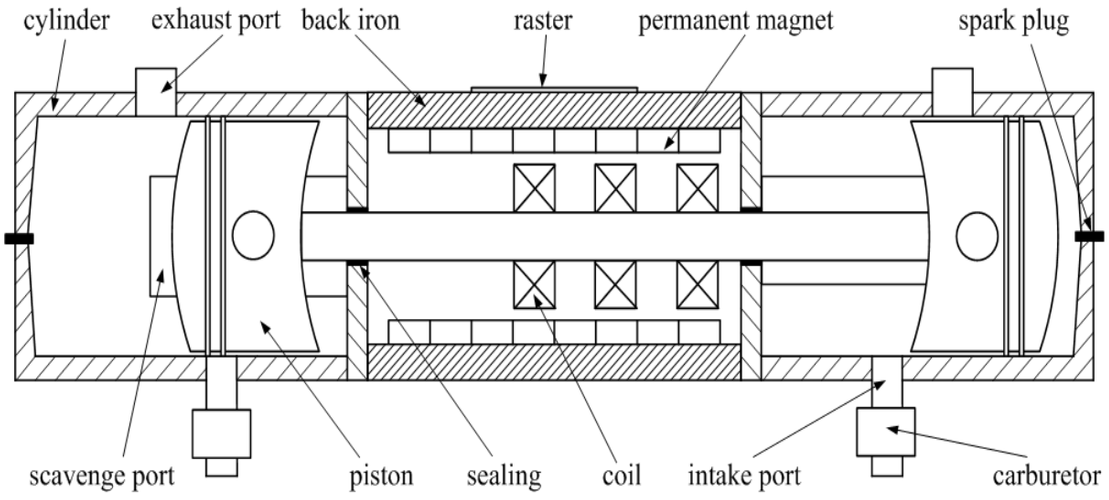


Fig. 1. FPLA configuration

## 2. System modeling

### 2.1 Dynamic modeling

The Modeling of FPLA and numerical simulation of its performance have already been done by a lot of researchers. Usually the model consists of a dynamic calculation of the piston motion and a thermodynamic calculation of the engine's thermodynamic events. The piston motion is governed by the interaction of forces that act on the piston simultaneously, which are in-cylinder pressure force from each cylinder, electromagnetic force, friction force and inertia force, as is shown in Fig.2.

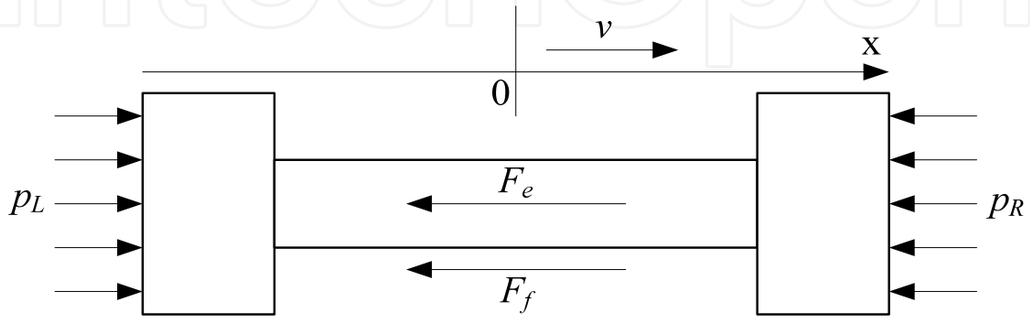


Fig. 2. Free body diagram for FPLA

The Newton's second law is applied:

$$m\frac{d^2x}{dt^2} = \left(p_L - p_R\right)A - F_f - F_e \tag{1}$$

Since the FPLA doesn't have a crankshaft, it is free of the dynamic friction caused by the crankshaft mechanism and the friction force is caused mainly by the interactions between cylinder and piston rings, cylinder and piston skirt, which is small compared with the load of the linear alternator. Therefore, the friction force is considered to be constant during the whole cycle in the calculation [13].

### 2.2 Modeling of the linear alternator

The linear alternator consists of two main components, a stator and a translator. The permanent magnets are mounted on the stator and the translator is the moving portion of the machine which is made up of coils. A schematic of a three-phase, "U" shaped linear alternator with permanent magnet (PM) excitation is shown in Fig.3.

The FPLA operates on the same basic physical principles as conventional rotary alternators. The principle that governs the voltage generating operation of the alternator is Faraday's law expressed as [14]:

$$\varepsilon_{ind} = -\frac{d\lambda}{dt} = -N_{coil}\frac{d\phi}{dt} \tag{2}$$

The permanent magnets create a magneto motive force (MMF) in the air gap between the stator and the winding coils as shown in Fig.4, and it can be described by the following mathematic equation:

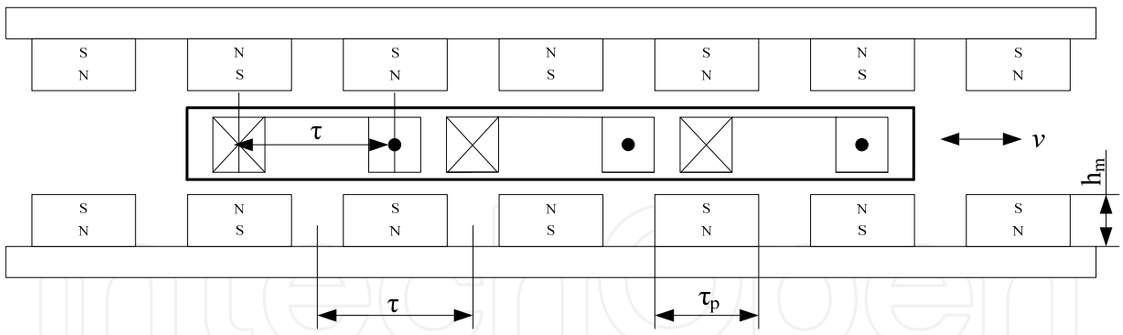


Fig. 3. Schematic of a U shaped three-phrase linear alternator

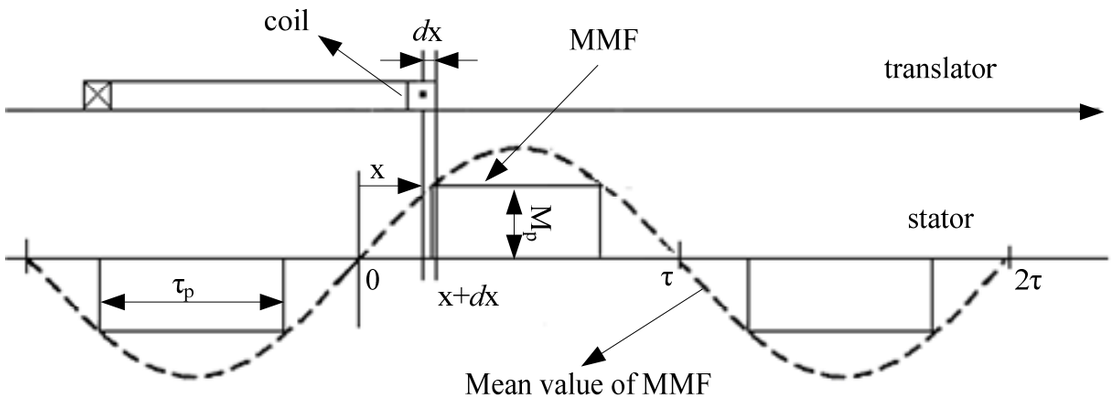


Fig. 4. Model of the linear alternator

$$M_F(x)=\begin{cases}0 & 0<x<\dfrac{\tau-\tau_p}{2}\\ M_p & \dfrac{\tau-\tau_p}{2}<x<\dfrac{\tau+\tau_p}{2}\\ 0 & \dfrac{\tau+\tau_p}{2}<x<\dfrac{3\tau-\tau_p}{2}\\ -M_p & \dfrac{3\tau-\tau_p}{2}<x<\dfrac{3\tau+\tau_p}{2}\\ 0 & \dfrac{3\tau+\tau_p}{2}<x<2\tau\end{cases} \tag{3}$$

Where $M_p = H_c \cdot h_m$.

The mean value of the MMF can be obtained from the single-order truncated Fourier series [15]:

$$M_F(x)=\frac{a_0}{2}+a_1\cos\left(\frac{\pi x}{\tau}\right)+b_1\sin\left(\frac{\pi x}{\tau}\right) \tag{4}$$

Where,

$$a_0 = \frac{1}{\tau}\int_0^{2\tau} M_F(x)dx = 0$$

$$a_1 = \frac{1}{\tau}\int_0^{2\tau} M_F(x)\cos\left(\frac{\pi x}{\tau}\right)dx = 0$$

$$b_1 = \frac{1}{\tau}\int_0^{2\tau} M_F(x)\sin\left(\frac{\pi x}{\tau}\right)dx = \frac{4}{\pi}M_p \sin\left(\frac{\pi\tau_p}{2\tau}\right)$$

Then

$$M_F(x) = \frac{4}{\pi}M_p \sin\left(\frac{\pi\tau_p}{2\tau}\right)\sin\left(\frac{\pi x}{\tau}\right).$$

So the flux density in the air gap due to PM is:

$$B(x) = \frac{\mu_0}{g}M_F(x) = \frac{\mu_0}{g}\frac{4}{\pi}M_p \sin\left(\frac{\pi\tau_p}{2\tau}\right)\sin\left(\frac{\pi x}{\tau}\right) = B_m \sin\left(\frac{\pi x}{\tau}\right) \tag{5}$$

Where

$$B_m = \frac{\mu_0}{g}\frac{4}{\pi}M_p \sin\left(\frac{\pi\tau_p}{2\tau}\right).$$

Both experimental measurements and numerical calculation by finite element method showed that the flux in the air gap of the PM exited linear alternator in Fig.4 could be assumed to be sinusoidal supporting the above result [16].
Therefore, the flux contained in the differential element *dx* is:

$$d\phi = B(x)dA = B(x)Hdx \tag{6}$$

Then the total flux contained in the coil of one phase at random position *x* is described by the following equation:

$$\begin{aligned}\lambda(x) &= \int_{x-\tau}^{x} N_{coil}HB(x)dx = \int_{x-\tau}^{x} N_{coil}\frac{\mu_0}{g}\frac{4}{\pi}M_p \sin\left(\frac{\pi\tau_p}{2\tau}\right)\sin\left(\frac{\pi x}{\tau}\right)dx \\ &= -\tau H N_{coil}M_p \frac{\mu_0}{g}\frac{8}{\pi^2}\sin\left(\frac{\pi\tau_p}{2\tau}\right)\cos\left(\frac{\pi}{\tau}x\right)\end{aligned} \tag{7}$$

Thus, the induced electromotive force produced in the coil of one phase is:

$$\varepsilon = -\frac{d\lambda}{dt} = HN_{coil}M_p \frac{\mu_0}{g}\frac{8}{\pi}\sin\left(\frac{\pi\tau_p}{2\tau}\right)\sin\left(\frac{\pi}{\tau}x\right)\frac{dx}{dt} \tag{8}$$

The induced current from the load circuit can be derived in the following equations:

$$\varepsilon(t) = (R_s + R_L) i_L(t) + L\frac{di_L(t)}{dt} \tag{9}$$

$$i_L(t) = \frac{\varepsilon(t)}{R_s + R_L}\left(1 - e^{-\frac{R_s+R_L}{L}t}\right) \tag{10}$$

The magnetic force has the opposite direction to the direction of the translator's movement. According to Ampere's law, it is described in the following equation:

$$F_e = 2N_{coil}B(x)i_L H = 4H^2 N_{coil}^2 B_m^2 \frac{\left(1 - e^{-\frac{R_s+R_L}{L}t}\right)}{R_s + R_L}\sin^2\left(\frac{\pi x}{\tau}\right)\frac{dx}{dt} \tag{11}$$

When it comes to three-phase linear alternator, the third phase is derived from another two according to the following equation [17]:

$$\sin\varphi = -\sin\left(\varphi + \frac{2}{3}\pi\right) - \sin\left(\varphi - \frac{2}{3}\pi\right) \tag{12}$$

So the total electromagnetic force produced by a three-phase linear alternator is:

$$\begin{aligned} F_e &= 4H^2 N_{coil}^2 B_m^2 \frac{\left(1 - e^{-\frac{R_s+R_L}{L}t}\right)}{R_s + R_L}\frac{dx}{dt}\left(\sin^2\left(\frac{\pi x}{\tau} - \frac{2}{3}\pi\right) + \sin^2\left(\frac{\pi x}{\tau}\right) + \sin^2\left(\frac{\pi x}{\tau} + \frac{2}{3}\pi\right)\right) \\ &= 6H^2 N_{coil}^2 B_m^2\left(1 - e^{-\frac{R_s+R_L}{L}t}\right)\frac{1}{R_s + R_l}\frac{dx}{dt} \\ &= M\left(1 - e^{-\frac{R_s+R_L}{L}t}\right)\frac{dx}{dt} \end{aligned} \tag{13}$$

Where

$$M = 6H^2 N_{coil}^2 B_m^2 \frac{1}{R_s + R_l}$$

In order to develop a first approach analysis, it's assumed that the alternator circuit works in resonance condition, which means that the current and voltage have the same phase, so that it is possible to consider the circuit as only a resistance [18]. Thus, the electromagnetic force is proportional to the speed of the translator:

$$F_e = M\frac{dx}{dt} \tag{14}$$

### 2.3 Thermodynamic modeling

The thermodynamic model is derived based on the first law of thermodynamics and ideal gas law. It consists of the calculation of the process of scavenging, compression, combustion, expansion and exhaust. The zero-dimensional, single zone model is used to describe the thermodynamic process.

Appling the first law of thermodynamics and ideal gas law on the cylinder as an open thermodynamic system, shown in Fig.5, and assuming that the specific heat $c_V$ and the gas constant $R$ are constant:

$$\frac{dU}{dt} = -p\frac{dV}{dt} + \frac{dQ}{dt} + \dot{H}_i - \dot{H}_e \tag{15}$$

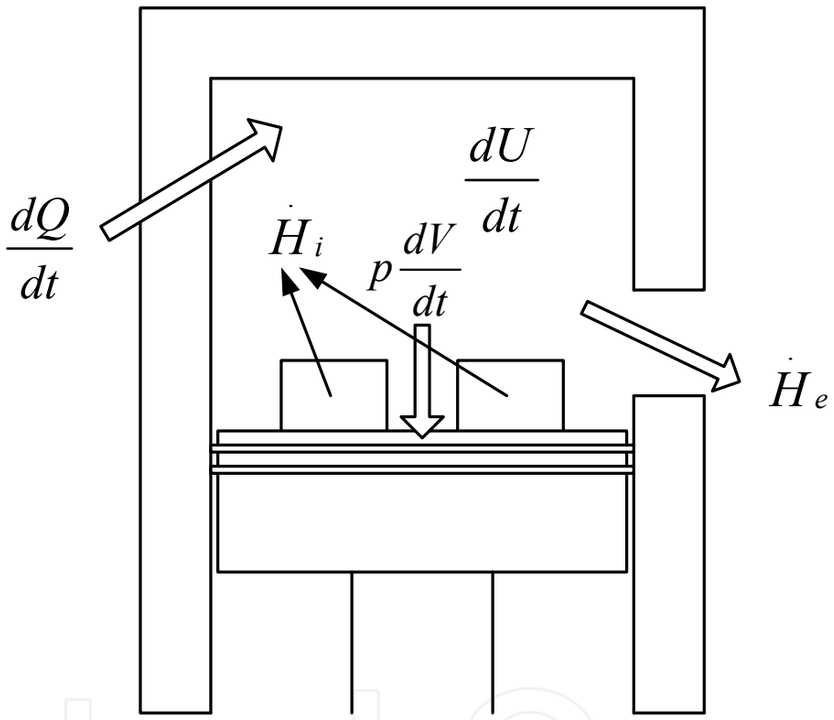


Fig. 5. Thermodynamic system of FPLA

For the case of compression and expansion process neglecting the crevice flow and the leakage, the first law of thermodynamics applied to the cylinder content becomes:

$$m_{in}\frac{d(c_V T)}{dt} = -p\frac{dV}{dt} + \frac{dQ}{dt} \tag{16}$$

Considering the cylinder content is ideal gas, and then at every instant the ideal gas law is satisfied:

$$pV = m_{in}RT \tag{17}$$

Substitution and mathematical manipulation yield the following equation which is used to calculate the in-cylinder pressure at each time step.

$$\frac{dp}{dt} = \frac{\gamma - 1}{V}\frac{dQ}{dt} - \gamma\frac{p}{V}\frac{dV}{dt} \tag{18}$$

In the combustion model, since the engine is crankless, a time-based Wiebe functions (as opposed to a conventional crank angle-based approach) is used to express the mass fraction burned in combustion process [4]:

$$\chi(t) = 1 - \exp\left[-a\left(\frac{t - t_0}{t_c}\right)^{1+b}\right] \tag{19}$$

and the heat rate released during combustion is:

$$\frac{\partial Q_c}{\partial t} = Q_{in}\frac{\partial \chi(t)}{\partial t} = Q_{in}\frac{1}{t_c}a(1+b)\left(\frac{t - t_0}{t_c}\right)^{b}\exp\left[-a\left(\frac{t - t_0}{t_c}\right)^{1+b}\right] \tag{20}$$

The in-cylinder heat transfer effect is modeled according to Hohenberg [19]:

$$\frac{\partial Q_{ht}}{\partial t} = hA_{cyl}\left(T - T_w\right) \tag{21}$$

$$h = 130V^{-0.06}\left(\frac{p}{10^5}\right)^{0.8}T^{-0.4}\left(\bar{U} + 1.4\right)^{0.8} \tag{22}$$

Since most heat transfer models, like the ones proposed by Woschni and Hohenberg, are made for Diesel engines. This means that they take radiative heat transfer effect into account, which is hardly present in premixed combustion. Hence, in the numerical simulations a factor of 0.5 is introduced to reduce the heat transfer coefficient [9].
So the total energy that is used to increase the in-cylinder pressure in equation (18) can be expressed in the following equation:

$$\frac{dQ}{dt} = \frac{\partial Q_c}{\partial t} - \frac{\partial Q_{ht}}{\partial t} \tag{23}$$

Exhaust blown down is modeled to be a polytrophic expansion process while the exhaust port is opening and the scavenging ports are still covered by the piston [11].

$$\frac{dp}{dt} = \frac{n - 1}{V}\frac{dQ}{dt} - n\frac{p}{V}\frac{dV}{dt} \tag{24}$$

For two-stroke spark ignition engines with under piston or crankcase scavenging, the scavenging efficiency is about 0.7~0.9 [20], , a scavenging efficiency of 0.8 is introduced to evaluate the effects of incomplete scavenging effect. The moment the scavenging ports are open, the pressure and temperature are assumed to be the same with the scavenging conditions and the incoming gases mix entirely with the burned gases.

## 3. Dimensionless analysis

### 3.1 Dimensionless modeling of FPLA

The dimension of a physical quantity is associated with combinations of mass, length, time, temperature and heat quantity, represented by symbols [M], [L], [T], [θ] and [H] respectively, each raised to rational powers. Since heat quantity is also a kind of energy, its dimension is replaced with $[ML^2T^{-2}]$.

The basic variables that involved were defined based on the dynamic and thermodynamic modeling of FPLA. The variables and their dimensions are listed in Tab.1.

| Variables | Symbol | Dimensions |
|---|---|---|
| Bore | $D$ | [L] |
| Piston area | $A$ | $[L^2]$ |
| Volume of the cylinder | $V$ | $[L^3]$ |
| Effective stroke length | $L_{eff}$ | [L] |
| Total stroke length | $L_{tot}$ | [L] |
| Translator ignition position | $x_{ign}$ | [L] |
| Mass of the translator | $m$ | [M] |
| Load coefficient | $M$ | $[MT^{-1}]$ |
| Friction force | $F_f$ | $[MLT^{-2}]$ |
| Energy | $Q$ | $[ML^2T^{-2}]$ |
| Scavenge pressure | $p_0$ | $[ML^{-1}T^{-2}]$ |
| Scavenge temperature | $T_0$ | [θ] |
| Pressure | $p$ | $[ML^{-1}T^{-2}]$ |
| Gas constant | $R$ | $[\theta L^{-1}T^{-2}]$ |
| Temperature | $T$ | [θ] |
| Wall temperature | $T_w$ | [θ] |
| Combustion duration | $t_c$ | [T] |
| Compression ratio | $\varepsilon$ | [1] |
| indicated efficiency | $\eta_i$ | [1] |
| Effective efficiency | $\eta_e$ | [1] |
| Time | $t$ | [T] |
| Frequency | $f$ | $[T^{-1}]$ |

Table 1. Basic variables and their dimensions

The effective stroke length is the distance between the upper edge of the exhaust port and the cylinder and the total stroke length is distance that the translator can travel from cylinder head to cylinder head [21].

Since the FPLA is controlled based on the displacement feedback of displacement sensor, the ignition timing is defined by the position of the translator where the controller gives out the ignition signals.

According to Buckingham's π theory [22], four fundamental reference variables which are independent from each other were chosen, and the other variables are described with these reference variables in their index form and every redefined variable is dimensionless. The four reference variables chosen were bore, mass of the translator, scavenging pressure and scavenging temperature.

Dividing the basic variables by the reference variables results in the dimensionless variables:

| | |
|---|---|
| Dimensionless bore | $D^*=D/D=1$ |
| Dimensionless piston area | $A^*=A/D^2$ |
| Dimensionless cylinder volume | $V^*=V/D^3$ |
| Dimensionless total stroke length | $L_{tot}{}^*= L_{tot}/D$ |
| Dimensionless mass of the translator | $m^*=m/m=1$ |
| Dimensionless scavenge air pressure | $p_0{}^*= p_0/p_0=1$ |
| Dimensionless scavenging temperature | $T_0{}^*=T_0/T_0=1$ |
| Dimensionless temperature | $T^*=T/T_0$ |
| Dimensionless wall temperature | $T_w{}^*=T_w/T_0$ |
| Dimensionless load coefficient | $M^*=M/(p_0{}^{0.5}D^{0.5}m^{0.5})$ |

Since the dimensionless translator ignition position is changing with different stroke length and fixed translator ignition position, in the dimensionless calculation, its actual dimensionless value taken is defined by the compression ratio the engine has already achieved when the spark plug ignites, as is described in Fig.6.

$$\varepsilon_{ign}=\frac{V_{eff}}{V_{ign}}=\frac{D^2L_{eff}}{D^2\left(L_{tot}/2-x_{ign}\right)}=\frac{L_{eff}/D}{\left(L_{tot}/2-x_{ign}\right)/D}=\frac{L_{eff}{}^*}{L_{tot}{}^*/2-x_{ign}{}^*} \tag{25}$$

Then the dimensionless translator ignition position can be deduced:

$$x_{ign}{}^*=\frac{L_{tot}{}^*}{2}-\frac{L_{eff}{}^*}{\varepsilon_{ign}} \tag{26}$$

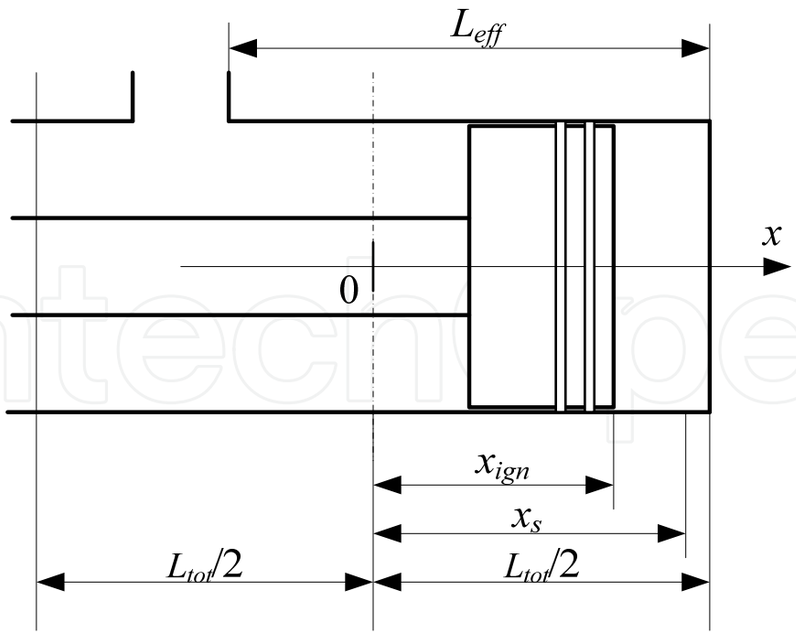


Fig. 6. Diagram of translator ignition position

Substituting all the dimensionless variables into equations (1) and (18), the following equations can be derived:

$$\frac{m}{m}\frac{d^2\left(\frac{x}{D}\right)}{d\left(\frac{t}{t_r}\right)^2}=\frac{1}{p_0}\frac{A}{D^2}\left(p_L-p_R\right)-\frac{1}{p_0D^2}F_f-\frac{M}{p_0^{\frac{1}{2}}D^{\frac{1}{2}}m^{\frac{1}{2}}}\frac{d\left(\frac{x}{D}\right)}{d\left(\frac{t}{t_r}\right)} \tag{27}$$

$$m^*\frac{d^2x^*}{dt^{*2}}=\left(p_L{}^*-p_R{}^*\right)A^*-F_f{}^*-M^*\frac{dx^*}{dt^*} \tag{28}$$

$$\frac{dp^*}{dt^*}=\frac{d\left(\frac{p}{p_0}\right)}{\left(\frac{t}{t_r}\right)}=-\gamma\frac{\frac{p}{p_0}}{\frac{V}{D^3}}\frac{d\left(\frac{V}{D^3}\right)}{d\left(\frac{t}{t_r}\right)}+\frac{\gamma-1}{\frac{V}{D^3}}\frac{d\left(\frac{Q}{p_oD^3}\right)}{d\left(\frac{t}{t_r}\right)} \tag{29}$$

$$\frac{dp^*}{dt^*}=-\gamma\frac{p^*}{V^*}\frac{dV^*}{dt^*}+\frac{\gamma-1}{V^*}\frac{dQ^*}{dt^*} \tag{30}$$

Where $t_r=m^{\frac{1}{2}}p_0{}^{-\frac{1}{2}}D^{-\frac{1}{2}}$ and equations (28) (30) are the dimensionless form of the translator's dynamic and thermodynamic equations.

The dimensionless gas constant was deduced based on the ideal gas law:

$$R^*=\frac{p^*V^*}{m_{in}{}^*T^*}=\frac{\frac{p}{p_0}\frac{V}{D^3}}{\frac{m_{in}}{m}\frac{T}{T_0}}=\frac{mT_0}{p_0D^3}\frac{pV}{m_{in}T}=\frac{R}{\frac{p_0D^3}{mT_0}} \tag{31}$$

Since the in-cylinder temperature is strongly transient, the dimensionless in-cylinder temperature is acquired using the dimensionless ideal gas law:

$$T^*=\frac{p^*V^*}{m_{in}{}^*R^*} \tag{32}$$

So the dimensionless variables defined in equations (28) (30) and (31) are:

| | |
|---|---|
| Dimensionless time | $t^*=t/t_r$ |
| Dimensionless combustion duration | $t_c{}^*=t_c/t_r$ |
| Dimensionless frequency | $f^*=f\cdot t_r$ |
| Dimensionless friction force | $F_f^*=F_f/(p_0\cdot D^2)$ |
| Dimensionless pressure | $p^*=p/p_0$ |
| Dimensionless energy | $Q^*=Q/(p_0\cdot D^3)$ |
| Dimensionless gas constant | $R^*=R/(p_0\cdot D^3/m/T_0)$ |

The combustion model and heat transfer equations can also be transferred to their dimensionless form using the dimensionless parameters we have already obtained:

$$\frac{\partial Q_c{}^*}{\partial t^*}=Q_{in}{}^*\frac{a(b+1)}{t_c^*}\left(\frac{t^*-t_0^*}{t_c^*}\right)^b\exp\left[-a\left(\frac{t^*-t_0^*}{t_c^*}\right)^{b+1}\right] \tag{33}$$

$$h^* = 130V^{*-0.06}\left(\frac{p^*}{10^5}\right)^{0.8} T^{*-0.4}\left(\bar{U}^* + 1.4\right)^{0.8} \tag{34}$$

$$\frac{\partial Q_{ht}^*}{\partial t^*} = h^* A_{cyl}^* \left(T^* - T_w^*\right) \tag{35}$$

All the equations were solved with a numerical simulating program in Matlab. The program starts calculation using a group of mathematic equations describing the dimensionless dynamic and dimensionless thermodynamic processes of FPLA, including the heat transfer rate, the in-cylinder pressure, the in-cylinder temperature, the fraction of fuel that burnt, the load and the work done, etc. At each time step, the program calls the dynamic subroutine and updates the displacement, the velocity, the averaged velocity and the acceleration. After the engine stabilizes, the program calculates the engine frequency, the compression ratio, the indicated power, the frictional power, the effective power output and the effective efficiency.

The dimensionless form of the output parameters are:

Dimensionless compression ratio $\varepsilon^* = \dfrac{L_{eff}^*}{L_{tot}^*/2 - x_s^*} = \dfrac{L_{eff}}{L_{tot}/2 - x_s} = \varepsilon$

Dimensionless frictional work $W_f^* = 4F_f^* x_s^*$

Dimensionless averaged speed $\bar{U}^* = 4x_s^* f^*$

Dimensionless indicated work $W_i^* = \oint_{V^*} p^* dV^*$

Dimensionless effective work $W_e^* = W_i^* - W_f^*$

Dimensionless indicated efficiency $\eta_i^* = \dfrac{W_i^*}{Q_{in}^*} = \dfrac{W_i}{Q_{in}} = \eta_i$

Dimensionless effective efficiency $\eta_e^* = \dfrac{W_i^* - W_f^*}{Q_{in}^*} = \dfrac{W_i - W_f}{Q_{in}} = \eta_e$

Dimensionless effective power output $P_e^* = W_e^* f^*$

Dimensionless frictional power $P_f^* = W_f^* f^*$

The dimensionless compression ratio and efficiency have just the same value with their dimensional forms, which are used to validate the correctness of the dimensionless process.

### 3.2 Operating ranges

The variables of the dimensionless analysis were chosen to cover the normal operating ranges of two-stroke free-piston engine. The base case represented the parameters of the experimental spark ignited, two-stroke FPLA prototype that was built in Beijing Institute of Technology. The basic parameters are listed in Tab.2.

The effective stroke length to bore ratio, dimensionless load coefficient, dimensionless translator ignition position, dimensionless combustion duration and dimensionless input

energy (opening proportion of the throttle) were the variable input factors of the parametric study. The dimensionless operating matrixes of each parameter are listed in Tab.3.

| Basic parameters | Value | Dimensionless value |
|---|---|---|
| $D$/mm | 34 | 1 |
| $L_{\text{eff}}$/mm | 20 | 0.5882 |
| $L_{tot}$/mm | 36 | 1.0588 |
| $R_l$/Ω | 2.5 | × |
| $R_s$/Ω | 2 | × |
| $M$/N·(m·s$^{-1}$)$^{-1}$ | 55.3 | 0.7746 |
| $m$/kg | 1.74 | 1 |
| $p_0$/bar | 1 | 1 |
| $T_0$/K | 293 | 1 |
| $T_w$/K | 453 | 1.5461 |
| $t_c$/ms | 5 | 0.2210 |
| $\varepsilon_{\text{ign}}$ | 4 | × |
| $a$ | 30% | × |

Table 2. Parameters of the FPLA prototype

| Parameters | Value | | | | | | |
|---|---|---|---|---|---|---|---|
| | case1 | case2 | case3 | case4 | case5 | case6 | case7 |
| $L_{eff}^*$ | 0.5 | 0.6 | 0.7 | 0.8 | 0.9 | 1.0 | 1.1 |
| $R_L$/Ω | 2 | 2.5 | 3 | 4 | × | × | × |
| $M$/N·(m·s$^{-1}$)$^{-1}$ | 62.2320 | 55.3174 | 49.7856 | 41.4880 | × | × | × |
| $M^*$ | 0.8714 | 0.7746 | 0.6971 | 0.5809 | × | × | × |
| $\varepsilon_{ign}$ | 3 | 4 | 5 | 6 | × | × | × |
| $t_c$/ms | 3 | 4 | 5 | 6 | × | × | × |
| $t_c^*$ | 0.1326 | 0.1768 | 0.2210 | 0.2652 | × | × | × |
| $a$ | 25% | 30% | 35% | × | × | × | × |

Table 3. Dimensionless operating matrix of FPLA

The dimensionless effective stroke length was defined as the first independent variable while the dimensionless load coefficient, dimensionless translator ignition position, dimensionless combustion duration and dimensionless input energy were taken as second independent variables. When analyzing the effects of each second variable, the other second variables would be set to equal to the base case which was decided by the FPLA prototype.

## 4. CFD calculation of combustion process for validation

### 4.1 Combustion modeling of FPLA

Since the combustion model used in the numerical program is zero dimensional Wiebe function and some parameters like combustion duration are of great uncertainty, the accuracy of the numerical calculated results is suspectable. Nowadays, multi-dimensional CFD computational tools have become an integral part of the engine design process due mainly to advances in computing capabilities and improvements in the modeling techniques utilized. In this study, in order to validate the results of dimensionless analysis, a multi-

dimensional commercial CFD software AVL_Fire was used to evaluate the effects of translator ignition position with different effective stroke length to bore ratio.

As the FPLA doesn't have a crankshaft mechanism, the dynamics of the piston is totally different from conventional engine. The dynamics were defined based on the results of a zero dimensional FPLA modeling mentioned in the former paragraphs. The dynamics and thermodynamics equations of FPLA in section 2 were solved using a numerical simulating program in Matlab, and some of the parameters were defined according to the experimental data measured. Then the dynamics of the FPLA were incorporated into AVL_Fire to define the movement of the piston. The piston motion profile was described with two arrays of numbers, one of which represented the ECA (Here ECA is equivalent crank angle which is used to note the port timings. However, it is only a time notation since the free-piston engine does not have a crankshaft to define the piston's motion and $ECA = t \cdot f \cdot 360$ [23, 24, 25]) and the other represented the displacement of the piston, and then the file was imported into the CFD code directly. Since there was no coupling between CFD code and free piston's motion, the dynamics was adjusted depending on the desired operating frequency and the stroke of the free-piston engine in the zero-dimensional FPLA simulating program. The dynamic mesh tool *Fame Engine* in AVL_Fire was used to create the moving mesh according to the numerical simulated free-piston motion profile. The update of the volume was handled automatically at each time step based on the new positions of the piston.

Only compression, combustion and expansion processes of the free-piston engine were calculated in order to minimize the number of computational cells (intake port, scavenging ports, exhaust port and scavenging case were not included in the combustion process). The computational model of the cylinder is shown in Fig.7, and the basic geometry is defined based on the FPLA prototype. Due to the symmetry of the cylinder ports layout, it is only necessary to model half of the geometry in order to minimize the computational cost.

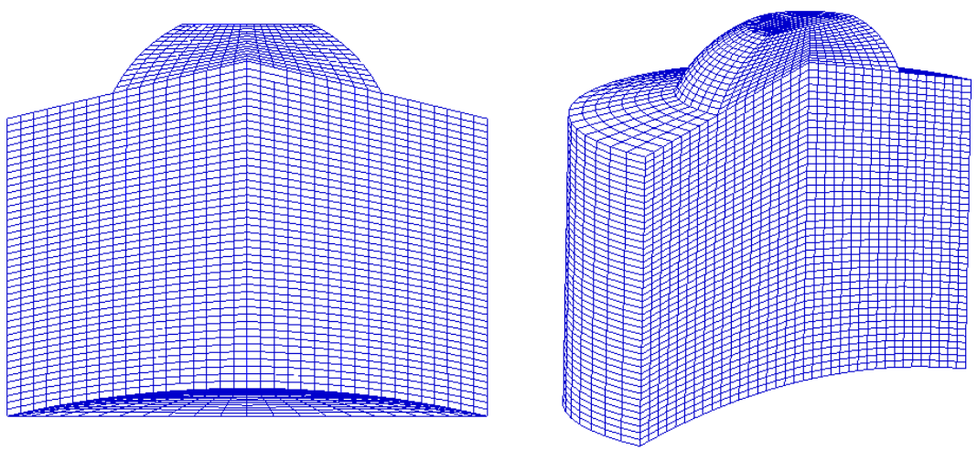

Fig. 7. Computational mesh of cylinder

### 4.2 Boundary conditions and combustion model

The boundary conditions were chosen to reflect the physical conditions which exist in the validation model and the prototype engine. Constant wall temperatures were also used. The standard $k$-$\varepsilon$ model was employed to capture turbulence. As the engine operates on a two

stroke cycle, the simulations run from the point of exhaust port closing to the point of exhaust port opening.

The initial conditions in the cylinder, such as pressure, temperature, EGR ratio and kinetic energy were defined based on the results of multi-dimensional scavenging calculation using CFD tools. In order to investigate the effects of ignition timings, the initial conditions were the same with base case. The input energy in the cylinder had just the same value as it is in the numerical simulation program.

Probability Density Function (PDF) model which takes into account the simultaneous effects of both finite rate chemistry and turbulence was chosen to describe the combustion process. The benefits of the PDF approach lie in the fact that it provides a complete statistical description of the scalar quantities under consideration. Thus, it allows first (mean values), second (variance), and even higher (skewness) order moments to be easily extracted, and that the term expressing the rate of chemical reaction appears in closed form.

### 4.3 CFD calculation cases

Based on the basic geometry of the FPLA, two kinds of effective stroke length to bore ratio and four ignition compression ratios were chosen in the CFD calculation. The other parameters are the same with the base case mentioned before.

As the piston dynamics is changing with different operating conditions, the piston motion profiles have to be defined first in the numerical simulation program, and then the required data in the CFD calculation can be derived, which are listed in Tab.4. The other parameters are based on the FPLA prototype. The revolution of the engine doesn't has real meanings as the free piston engine does not have a crankshaft, and it is bring forward just to complete the combustion process required by the CFD software.

Practically, the maximum compression ratio is confined by the geometry of the chamber since the roof of cylinder and piston is not flat, as is shown in Fig.7. Thus, we have to make sure that the compression ratios of the typical effective stroke length chosen do not exceed their maximum value.

| $L_{eff}$/mm | D/mm | $L_{eff}$ /D | $\varepsilon_{ign}$ | $t_{ign}$/ECA | $\varepsilon$ | $f$/Hz | EGR | $Q_{in}$/J | Revolution/rpm |
|---|---|---|---|---|---|---|---|---|---|
| 23 | 34 | 0.6765 | 3 | 319.5 | 21.0 | 46.7 | 20% | 17.84 | 2803.7 |
| 23 | 34 | 0.6765 | 4 | 328.5 | 22.2 | 45.0 | 20% | 17.84 | 2697.8 |
| 23 | 34 | 0.6765 | 5 | 333.6 | 21.6 | 43.4 | 20% | 17.84 | 2606.4 |
| 23 | 34 | 0.6765 | 6 | 337.4 | 20.7 | 42.2 | 20% | 17.84 | 2531.6 |
| 35 | 34 | 1.0294 | 3 | 320.7 | 11.4 | 34.1 | 20% | 27.15 | 2046.4 |
| 35 | 34 | 1.0294 | 4 | 328.6 | 13.8 | 33.7 | 20% | 27.15 | 2025.0 |
| 35 | 34 | 1.0294 | 5 | 333.7 | 14.6 | 33.0 | 20% | 27.15 | 1980.2 |
| 35 | 34 | 1.0294 | 6 | 335.4 | 14.5 | 32.1 | 20% | 27.15 | 1928.0 |

Table 4. CFD calculation cases

The piston motion profiles with different operating conditions listed in Tab.4 are shown in Fig.8.

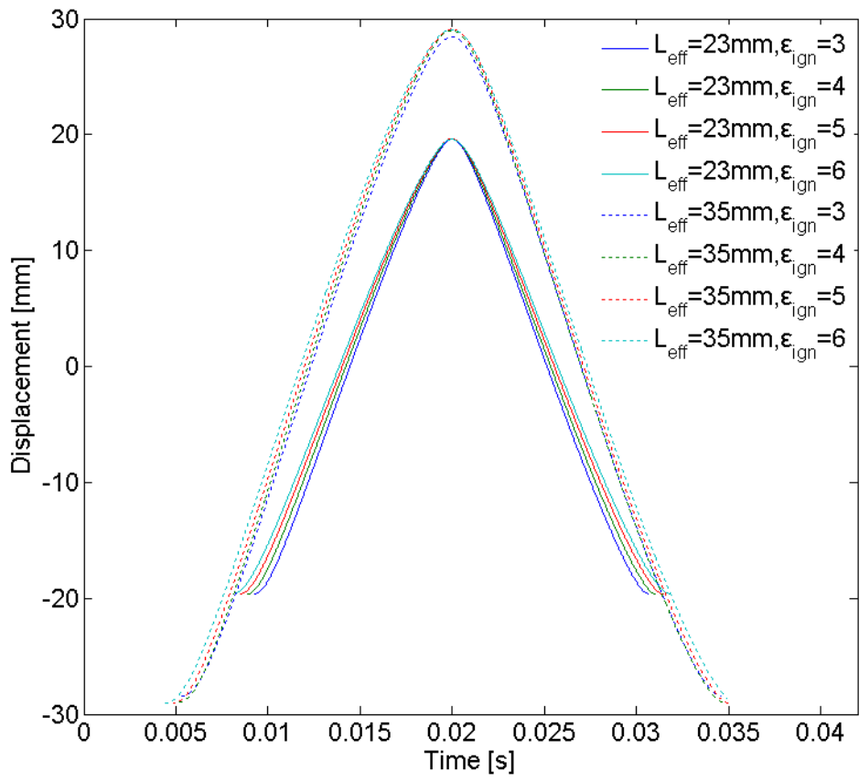


Fig. 8. Piston dynamics with different operating conditions

## 5. Results and discussion

### 5.1 Zero dimensional models validation

In order to make sure most part of the numerical simulation program is correct, the numerical simulated in-cylinder pressure is compared with experimental derived pressure in Fig.9. The thermodynamic model used in the numerical analysis is a single zone model. In single zone models the cylinder mixture composition, pressure and temperature are considered to be uniform and the energy release rate is modeled using experiential model. Matching the experimentally and numerically derived pressure profiles was a complicated task due to the simplification and unknown variables, such as the actual heat addition, the combustion duration and the actual load when the engine was running. Seen in Fig.9, the numerical simulation model used to simulate the operation of FPLA proved to be in agreement with the experimental data with a certain combination of the variables.

### 5.2 Effects of dimensionless parameters

#### 5.2.1 Effects of dimensionless effective stroke length

The stroke to bore ratio is one of the core design variables in internal combustion engines, relating combustion chamber surface area to its volume and piston area to stroke length [11]. In order to predict the performance of FPLA with various sizes and dimensions, seven cases of dimensionless effective stroke length were chosen as the basic variable to investigate the performance of the FPLA in wide operating ranges.

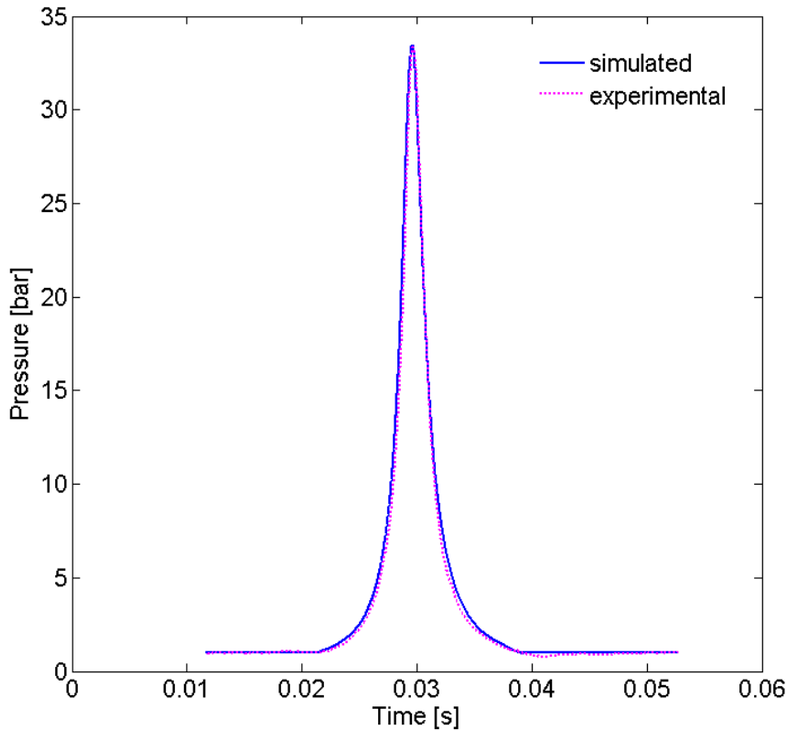


Fig. 9. Comparation of experimental and numerical simulated pressure data

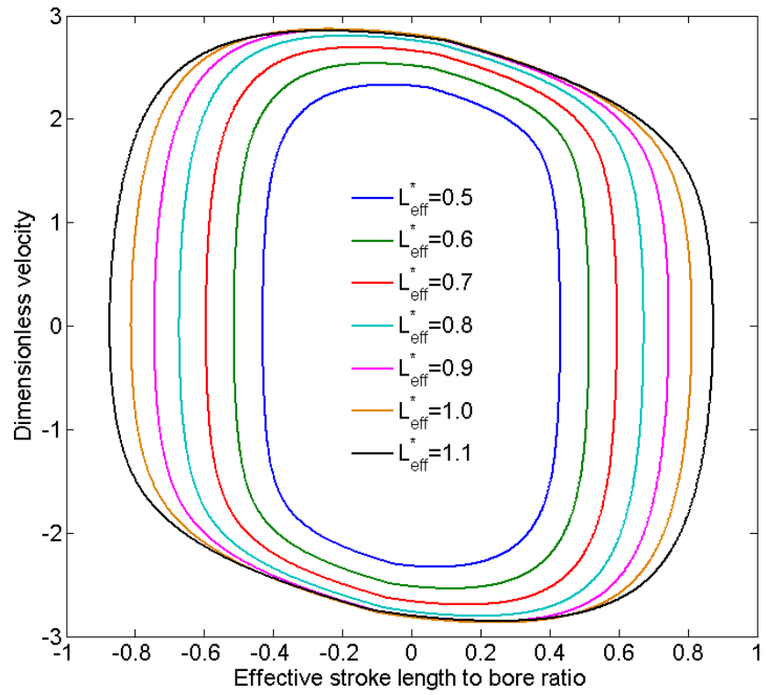


Fig. 10. Dimensionless velocity vs. dimensionless displacement with different effective stroke length to bore ratio

Fig.10 illustrates the change of dimensionless velocity versus dimensionless displacement for different effective stroke length to bore ratios while the other parameters remain the same with the base case. It can be seen that as the dimensionless effective stroke length increases, the dimensionless velocity increases. However, the profile of all the curves is similar to each other, which means this kind of free-piston engine has its own specific characteristics.

As is shown in Figs.11~13, the dimensionless compression ratio, dimensionless frequency and dimensionless in-cylinder peak pressure keep decreasing as the effective stroke length to bore ratio increases. These are because as the dimensionless effective stroke length increases, the translator has to travel longer strokes and more energy is wasted overcoming friction. And as the effective stroke length to bore ratio increases, the cylinder contains more charge and the charge would contain more energy during compression stoke; therefore the dimensionless compression ratio would decrease.

The highest dimensionless effective efficiency is achieved while $L_{eff}^*$ is 0.8 under the basic working conditions, and the peak point is mainly affected by the other four dimensionless parameters, which will be discussed in the following sections.

As the effective stroke length to bore ratio increases, the dimensionless energy input to the engine every cycle increases as a result of increasing the volume of the cylinder. Since the dimensionless effective power output is also strongly determined by the dimensionless frequency and dimensionless effective efficiency, the highest effective power output is achieved while $L_{eff}^*$ is 0.9 under the basic working conditions.

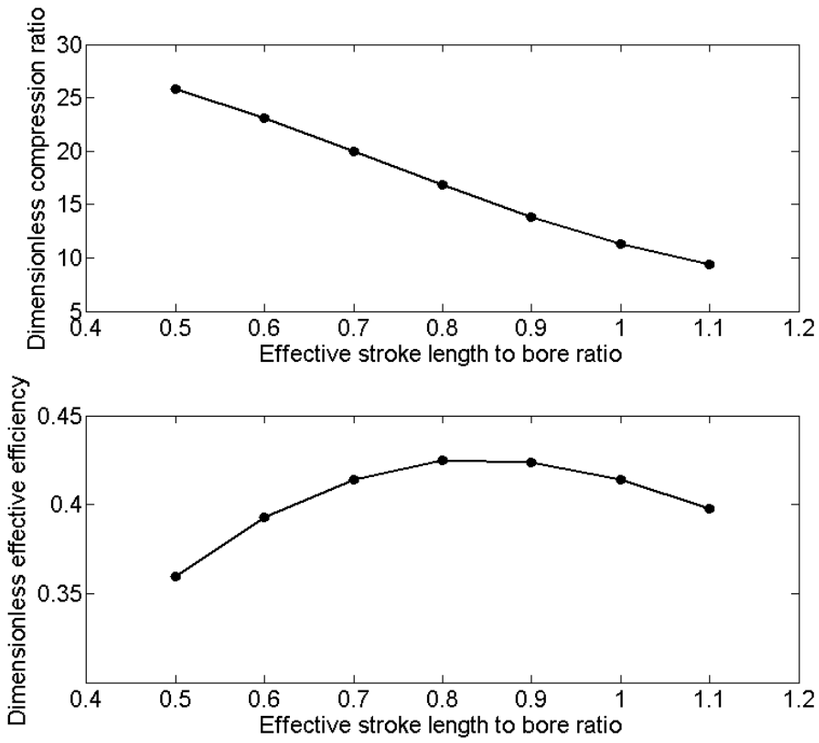


Fig. 11. Effects of effective stroke length to bore ratio to dimensionless compression ratio and dimensionless effective efficiency

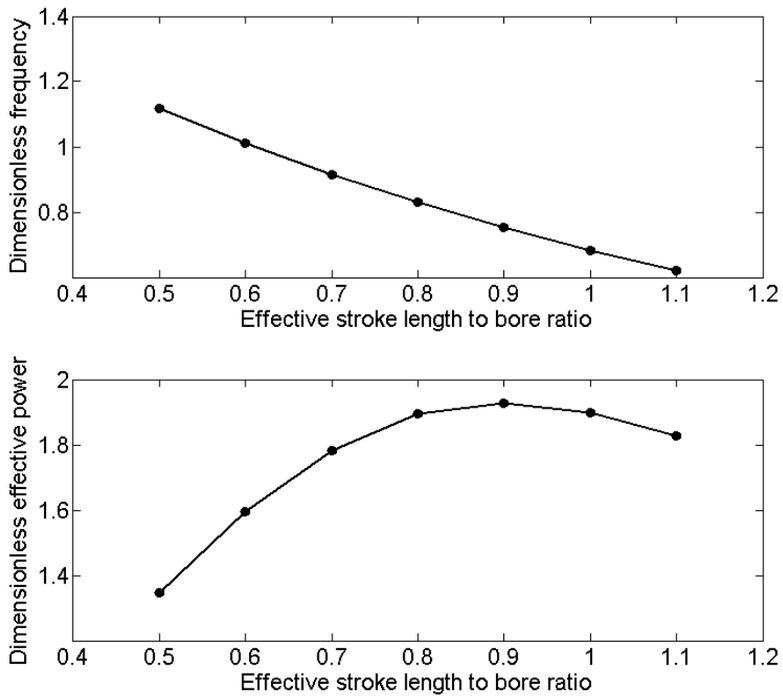


Fig. 12. Effects of effective stroke length to bore ratio to dimensionless frequency and dimensionless effective power output

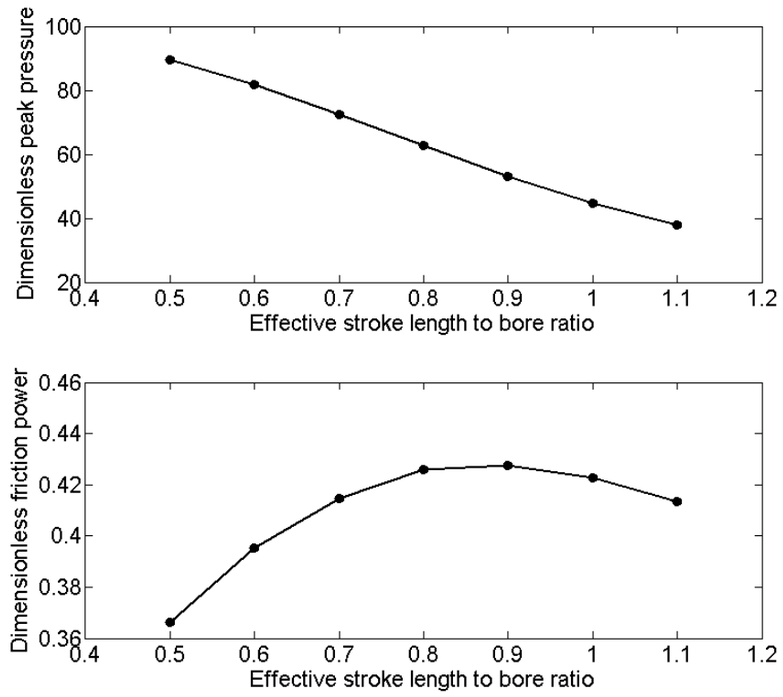


Fig. 13. Effects of effective stroke length to bore ratio to dimensionless peak pressure and dimensionless frictional power

### 5.2.2 Effects of dimensionless load coefficient

Increasing the dimensionless load coefficient means the load demand of the linear alternator is increasing and the electromagnetic force produced by the linear alternator is increasing. Four different dimensionless load coefficients ($M^*1>M^*2>M^*3>M^*4$) were chosen to investigate the effects of changing the load of the linear alternator. The load coefficient was varied by changing the value of the load resistance. According to the results calculated, the dimensionless load coefficient has large impact on different parameters studied and can affect the operating condition of FPLA.

According to Figs.14~15, as the dimensionless load coefficient increases, the dimensionless compression ratio and dimensionless frequency decrease since bigger electromagnetic force is acting on the translator. The highest dimensionless effective efficiency is changing with different dimensionless load coefficient and effective stroke length to bore ratio. As is shown in Fig.14, when the effective stroke length to bore ratio is less than 0.67, smaller dimensionless load coefficient would lead to a higher dimensionless effective efficiency and when the effective stroke length to bore ratio is more than 1.0, the larger the load coefficient the higher the dimensionless effective efficiency. The reason behind these is believed to be caused by the percentage of heat released before top dead center (TDC), which is strongly determined by the frequency of the translator.

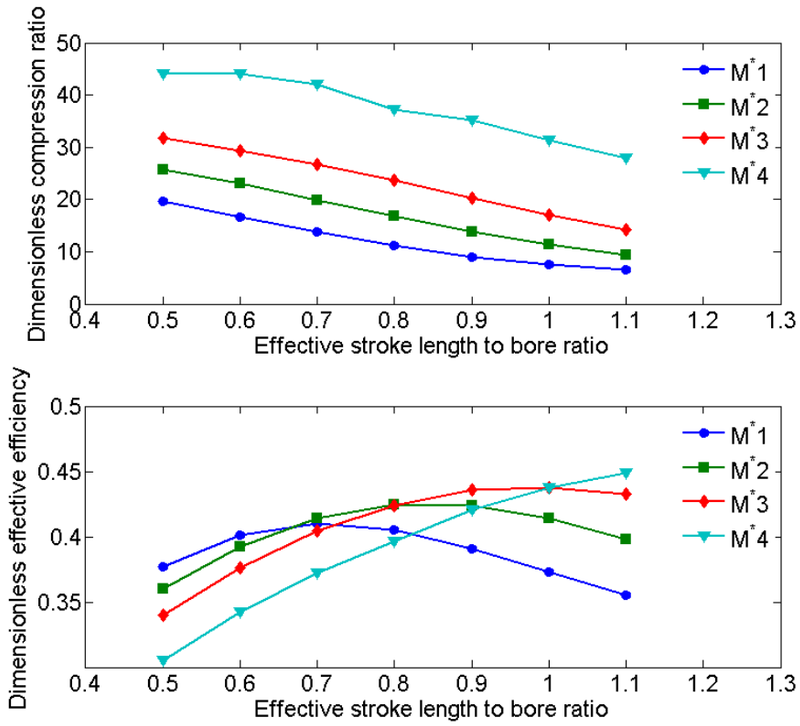


Fig. 14. Effects of dimensionless load coefficient to dimensionless compression ratio and dimensionless effective efficiency

As is shown in Fig.15, smallest dimensionless load coefficient lead to the highest dimensionless power output although the dimensionless effective efficiency is the lowest since the dimensionless frequency with smaller load coefficient is higher. It is more obvious when the effective stroke length to bore ratio is more than 1.0 since smaller load coefficient

lead to higher dimensionless effective efficiency and higher dimensionless frequency. Therefore, we can conclude that the main factor that controls the power output of FPLA is its frequency.

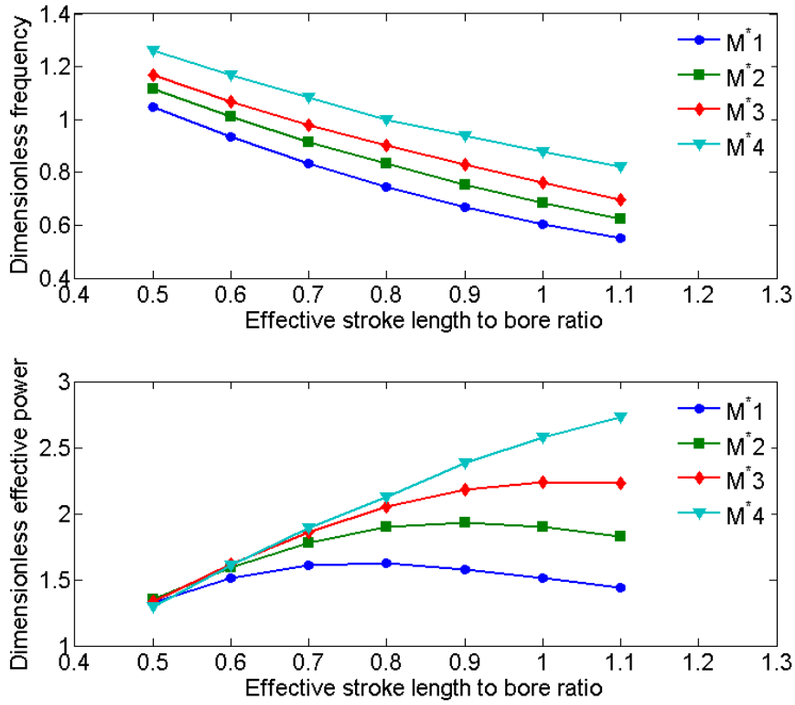


Fig. 15. Effects of dimensionless load coefficient to dimensionless frequency and dimensionless effective power output

### 5.2.3 Effects of dimensionless translator ignition position

Ignition timing is one of the major parameters that control the engine's operating conditions, such as frequency and compression ratio. Since the dimensionless ignition timing is changing with different dimensionless stroke length, the ignition timing is defined by the compression ratio the engine has already achieved when the spark plug ignites in the calculation, and it means that the lower the ignition compression ratio is the bigger the ignition advance is.

According to some literatures [3][5], it's held that an earlier combustion in diesel free-piston engines would lead to more waste of energy to reverse the translator, thus the efficiency and frequency would drop. However, according to the results of spark ignited FPLA obtained in this paper, with different effective stroke length to bore ratio the best ignition advance differs with each other, since an early ignition is associated with negative work in the compression stroke and a late ignition is associated with low peak in-cylinder pressure, as is shown in Fig.16.

As is described in Figs.17~18, with smaller effective stroke length to bore ratio (closer to 0.5), a bigger ignition advance would lead to higher dimensionless compression ratio, higher dimensionless effective efficiency, higher dimensionless frequency and higher dimensionless effective power output. The reason is that with small dimensionless effective

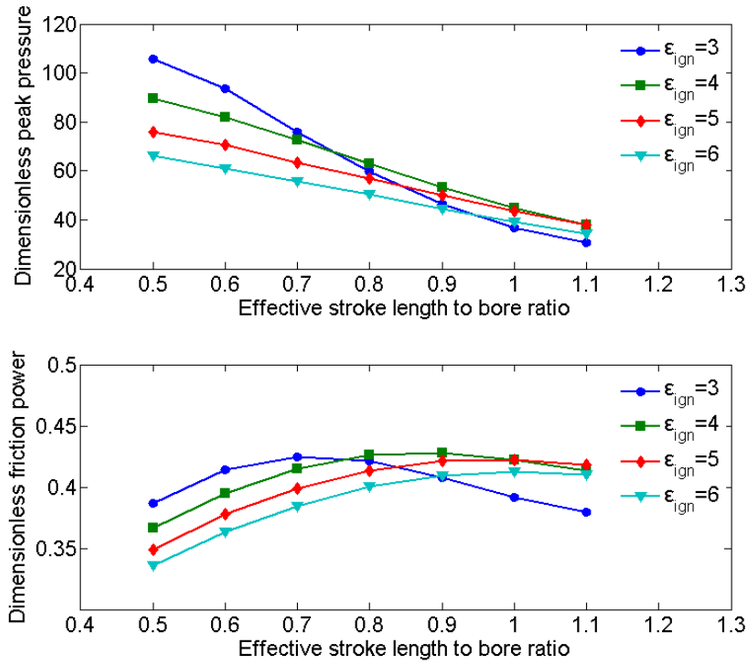


Fig. 16. Effects of dimensionless translator ignition position to dimensionless peak pressure and dimensionless frictional power

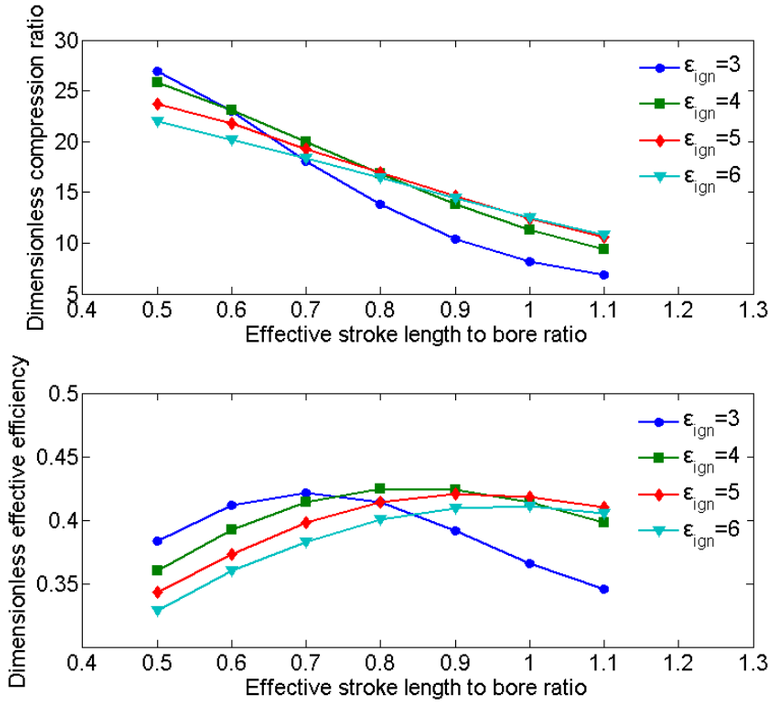


Fig. 17. Effects of dimensionless translator ignition position to dimensionless compression ratio and dimensionless effective efficiency

stroke length, the dimensionless frequency of FPLA is high and most of the energy is released after TDC. Thus, the in-cylinder peak pressure is higher with a bigger ignition advance, which will help improve the performance of the engine. With a high effective stroke length to bore ratio (closer to 1.1), the frequency of the engine decreases a lot since the translator has to travel a longer stroke and a bigger proportion of energy will be released before TDC, which is associated with negative work in the compression stroke. According to the results derived, when the dimensionless effective stroke length is longer than 1.0, the ignition compression ratio of 5 would leads to the best engine performance.

The dimensionless effective power output is determined by dimensionless effective efficiency and dimensionless frequency, as has been discussed before. As is shown in Fig.18, the biggest dimensionless power output is achieved when effective stroke length to bore ratio is 0.9 and ignition compression ratio is 4. Since the dimensionless frequency has little deviation with different ignition compression ratios, the dimensionless effective power output has similar trends with the dimensionless effective efficiency.

In order to analysis the effects of different ignition timings, the combustion duration was assumed to be invariant. However, the combustion duration is strongly depend on the working conditions of the engine, thus CFD tools were taken to analysis the effects of different ignition timings to verify the dimensionless results later.

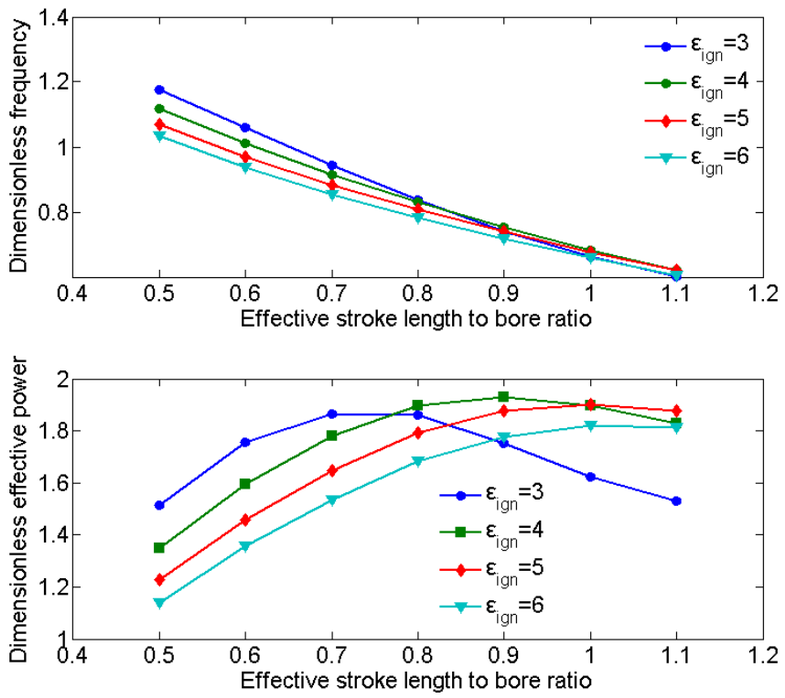


Fig. 18. Effects of dimensionless translator ignition position to dimensionless frequency and dimensionless effective power output

### 5.2.4 Effect of dimensionless combustion duration

The modeling of the heat release in free-piston engine is one of the factors with the highest degree of uncertainty in the simulation model [11]. The piston motion of free-piston engines

differs significantly from that of conventional engines and very little research exists on how this influences the combustion process. In the dimensionless calculation, the heat release rate is defined by the combustion duration and shorter combustion duration will lead to a faster heat release rate. Based on the base case, four cases of combustion duration were chosen to instigate its effects to the engine's performances.

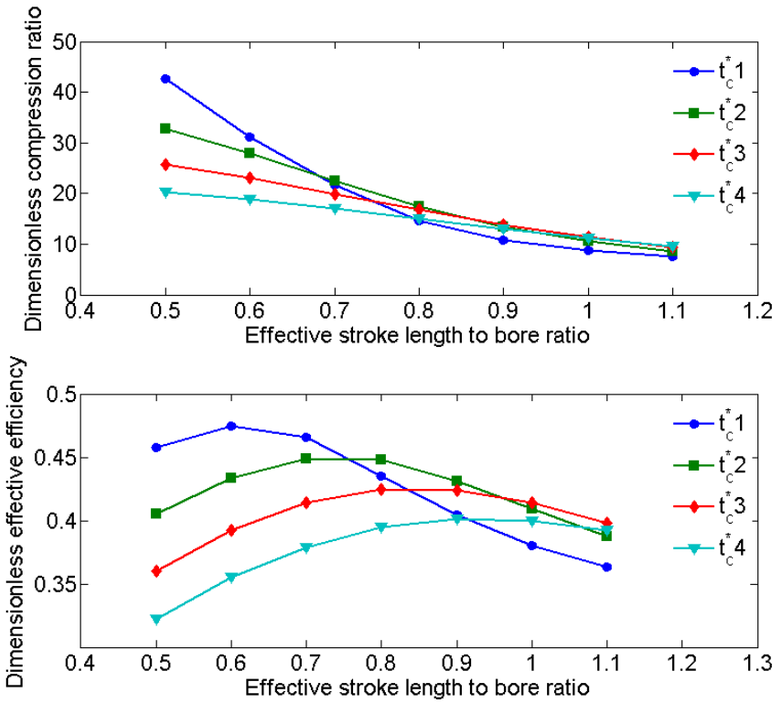


Fig. 19. Effects of dimensionless combustion duration to dimensionless compression ratio and dimensionless effective efficiency

Seen in Fig.19, a shorter combustion duration which means a faster heat release rate would lead to a higher compression ratio and higher effective efficiency when the dimensionless effective stroke length is less than 0.68 and 0.75. However, as the dimensionless effective stroke length increases, the dimensionless frequency will decrease and more energy will be released before TDC. For shorter combustion duration a lot more percentage of energy is released before TDC, which is associated with more negative work in the compression stroke. Thus, shorter combustion duration would lead to a lower dimensionless compression ratio and lower dimensionless effective efficiency with a longer dimensionless effective stroke length and fixed ignition compression ratio.

As is shown in Fig.20, shorter combustion duration leads to a higher frequency with smaller dimensionless effective stroke length and as dimensionless effective stroke length grows, shorter combustion duration leads to faster decreasing of dimensionless frequency as more energy is released before TDC to stop the translator. The dimensionless effective power output is determined by the dimensionless frequency and dimensionless effective efficiency and it has a similar trend with dimensionless efficiency.

Therefore, with a longer effective stroke length to bore ratio it is recommended to postpone the ignition timing to achieve a good performance of the free-piston engine.

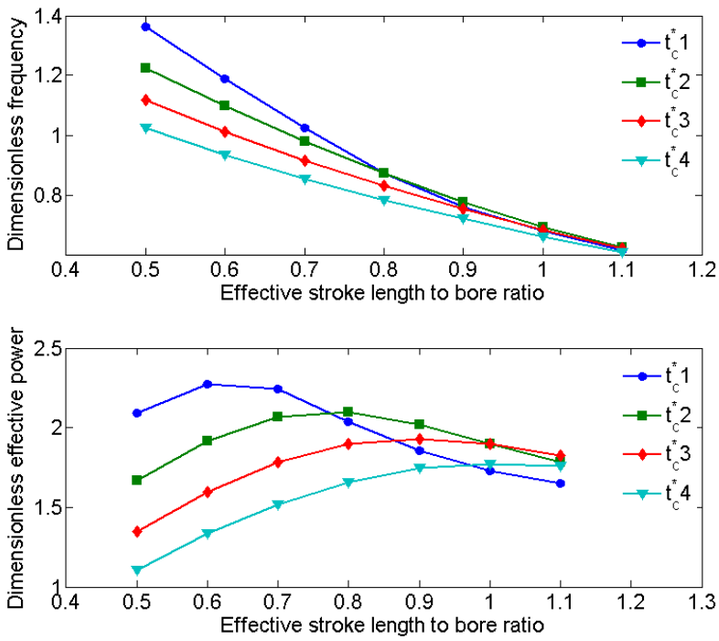


Fig. 20. Effects of dimensionless combustion duration to dimensionless frequency and dimensionless effective power output

### 5.2.5 Effects of dimensionless input energy

The free-piston engine investigated in this paper is a spark-ignited engine and the input energy is varied by changing the opening proportion of the throttle. For FPLA, a much narrow range of operating speeds is expected to be utilized, which is due to the electrical generating scheme employed by the device [23]. Therefore, the opening proportion of the throttle is confined to low speed range. According to the load of FPLA, efficient generation will be achieved by operation at a fixed oscillating rate.

The effects of different dimensionless input energy while other parameters remain the same with the base case are shown in Figs.21~22. As expected, with more input energy, the dimensionless frequency, dimensionless compression ratio and dimensionless effective power output of the engine are increasing since more energy is released in the combustion process.

The amount of energy input to the engine is strictly determined by the load of FPLA. If we keep increasing the amount of input energy, the current load coefficient is not suitable for the current load coefficient and the speed of the translator will keep increasing since extra energy cannot be extracted, and at last the piston will crush with the cylinder head, which is strictly forbidden. However, if we decrease the amount of input energy, the translator will stop since the amount of energy is not enough to sustain the stable operation of the engine. Therefore, the operation range of the engine is confined by the load of the linear alternator, and the amount of the input energy has to be adjusted with the load coefficient to obtain a higher efficiency or higher power output.

## 5.3 CFD calculated results

In order to verify the results of dimensionless translator ignition position of spark ignited free-piston engines, multi-dimensional CFD tools were used to calculate the combustion

process of the FPLA with four different ignition timings and two kinds of effective stroke length to bore ratio.

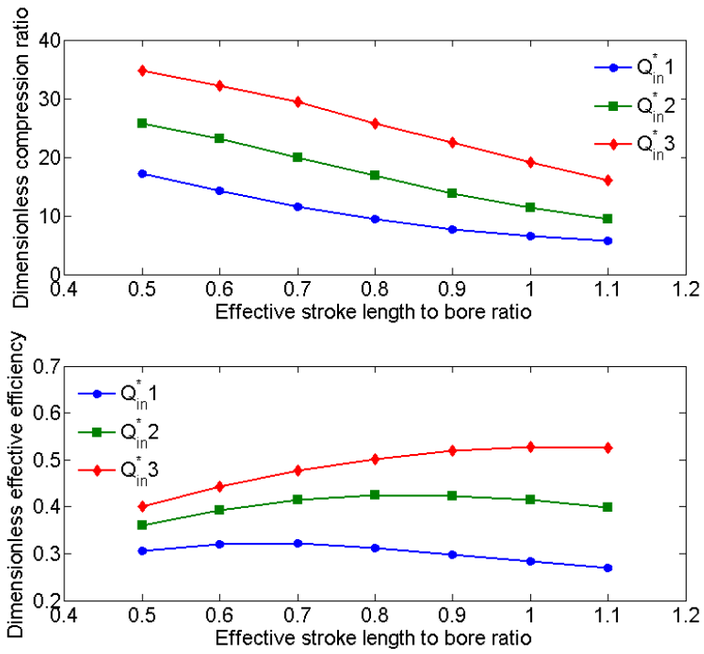


Fig. 21. Effects of dimensionless input energy to dimensionless compression ratio and dimensionless effective efficiency

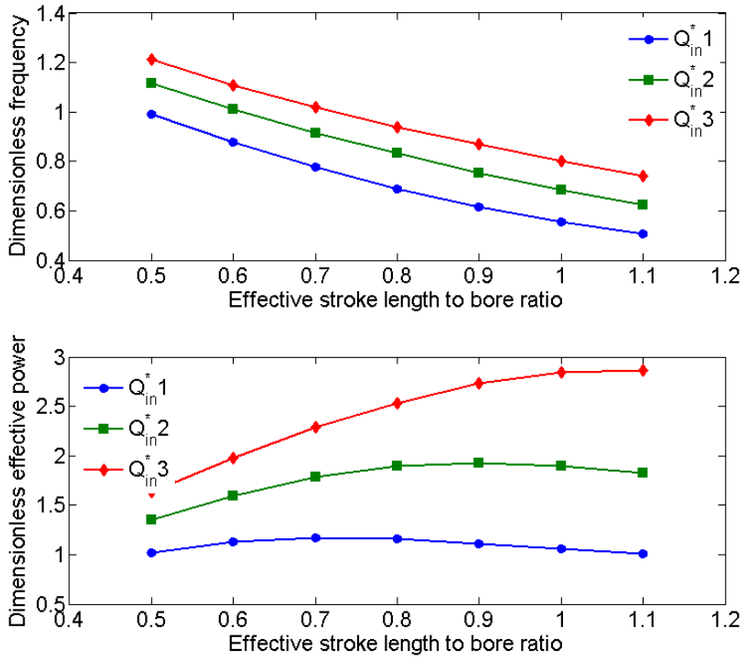


Fig. 22. Effects of dimensionless input energy to dimensionless frequency and dimensionless effective power output

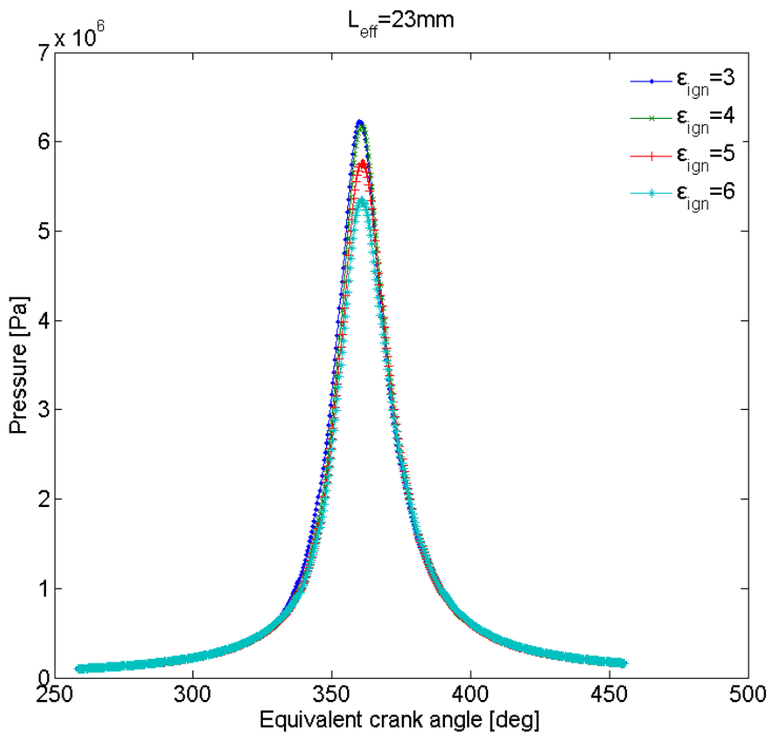


Fig. 23. In-cylinder pressure with different translator ignition position while $L_{eff}^{*}$=0.6765

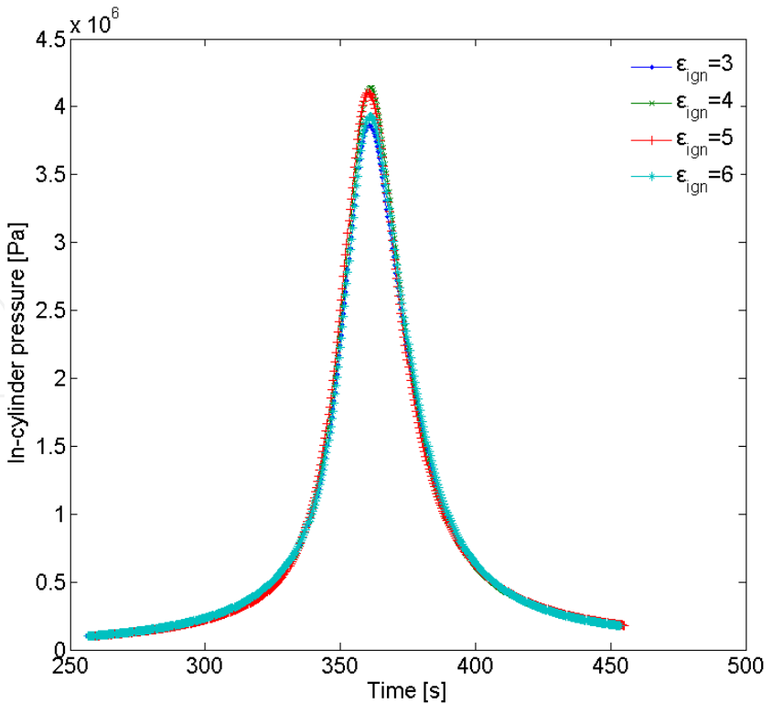


Fig. 24. In-cylinder pressure with different translator ignition position while $L_{eff}^{*}$=1.0294

**Nomenclature**

| | | | |
|---|---|---|---|
| $a$ | combustion constant | $R$ | air gas constant |
| $A$ | top area of the piston | $R_L$ | load resistance |
| $A_{cyl}$ | heat transfer area | $R_s$ | internal resistance of coils |
| $b$ | combustion form factor | $t$ | time |
| $B$ | magnetic induction intensity | $t_0$ | time combustion begins |
| $c_V$ | constant volume specific heat | $t_c$ | combustion duration |
| $D$ | cylinder diameter | $t_{ign}$ | ignition timing |
| $f$ | frequency | $T$ | temperature |
| $F_e$ | electromagnetic force | $T_0$ | scavenge temperature |
| $F_f$ | friction force | $T_w$ | wall temperature |
| $g$ | air gap length | $U$ | internal energy |
| $h$ | heat transfer coefficient | $\bar{U}$ | mean piston speed |
| $h_m$ | thickness of the permanent magnet | $V$ | displaced volume of the cylinder |
| $H$ | length of the coils cutting magnetic lines | $V_{eff}$ | effectively compressed volume of the cylinder |
| $H_c$ | magnetic field strength | $V_{ign}$ | volume of the cylinder when ignite |
| $H_e$ | enthalpy output | $W$ | work done |
| $H_i$ | enthalpy input | $W_e$ | effective work |
| $i_L$ | current in the load circuit | $W_f$ | frictional work |
| $L$ | induction | $W_i$ | indicated work |
| $L_{tot}$ | total stroke length | $x$ | displacement of the translator |
| $L_{eff}$ | effective stroke length | $x_{ign}$ | translator ignition position |
| $m$ | translator mass | $x_s$ | half of maximum stroke length |
| $m_{in}$ | mass of the charge | $a$ | opening proportion of throttle |
| $M$ | load coefficient | $\gamma$ | specific heat ratio |
| $M_F$ | mean magneto motive force | $\varepsilon$ | compression ratio |
| $n$ | polytrophic exponent | $\varepsilon_{ign}$ | ignition compression ratio |
| $N_{coil}$ | number of turns in the coil | $\varepsilon_{ind}$ | induced voltage |
| $p$ | in-cylinder absolute pressure | $\Phi$ | flux passing through the coil |
| $p_0$ | scavenge pressure | $\lambda$ | total flux pass through the coil |
| $p_L$ | pressures in the left cylinder | $\mu_0$ | vacuum permeability |
| $p_R$ | pressures in the right cylinder | $\tau$ | pole pitch |
| $P_e$ | effective power output | $\tau_p$ | width of PM |
| $P_f$ | frictional power | $\eta_e$ | effective efficiency |
| $Q$ | energy | $\eta_i$ | indicated efficiency |
| $Q_c$ | heat released in combustion | $\frac{dx}{dt}$ | velocity |
| $Q_{ht}$ | heat transfer | $\frac{d^2x}{dt^2}$ | acceleration |
| $Q_{in}$ | total input energy | | |

(The variable with superscript "*" is its dimensionless form.)

The in-cylinder pressure curves with different ignition compression ratio while $L_{eff}^*$=0.6765 are shown in Fig.23. It is clear that smaller ignition compression ratio or bigger ignition advance leads to higher peak pressure which is in agreement with the dimensionless results.

The in-cylinder pressure curves with different ignition compression ratio while $L_{eff}^{*}$=1.0294 are shown in Fig.24. The sequence of the peak pressure achieved with different ignition compression ratio is $p_{\varepsilon_{ign}=4} > p_{\varepsilon_{ign}=5} > p_{\varepsilon_{ign}=6} > p_{\varepsilon_{ign}=3}$, which supports the dimensionless results. The combustion duration calculated via CFD is about 4.4~5.6ms with different ignition timings and effective stroke length, which has some deviation with the value in numerical simulating program which is defined based on the heat release rate of FPLA prototype. The deviations can be eliminated by using an iterative procedure between the numerical simulating program and CFD calculation when calculating a specific free-piston engine.

## 6. Conclusion

A detailed dimensionless modeling and dimensionless parametric study of spark ignited FPLA was presented to build up a guideline for the design of FPLA prototype with desired operating performances. The parameters of the numerical simulation program were amended by comparing the simulated in-cylinder pressure with experimentally derived data. At last CFD calculation of the combustion process was carried out to verify the effects of translator ignition position with two kinds of typical effective stroke length to bore ratios. According to the dimensionless results, it can be concluded that:

1. For FPLA, a much narrow range of low operating speeds is expected to be utilized, which is due to the electrical generating scheme employed by the device. Therefore, a bigger stroke to bore ratio is favorable to decrease the to and fro frequency of the translator.
2. According to the load of FPLA, efficient power generation will be achieved by operating at a fixed oscillating rate. With smaller effective stroke length to bore ratio, bigger load coefficient is advantageous to achieve a higher effective efficiency while smaller load coefficient would lead to higher effective efficiency with bigger effective stroke length to bore ratio. Smaller load coefficient would lead to higher effective power output.
3. It has been found that an optimum ignition advance is available for the free-piston engine to achieve its best performance since earlier ignition is associated with more negative work in the compression stroke and a later ignition is associated with low peak in-cylinder pressures.
4. The efficiency of the engine is mainly associated with the proportion of the energy released before TDC which is associated with negative work to stop the translator. With a longer effective stroke length to bore ratio it is recommended to postpone the ignition timing to achieve a good performance of the engine.
5. According to the CFD calculated results with typical effective stroke length to bore ratio and ignition timings, the dimensionless results were reasonable.

## 7. References

[1] Hannson J, Leksell M, Carlesson F. Minimizing power pulsation in a free piston energy converter. Proceedings of the 11th European Conference on Power Electronics and Applications (EPE05), Dresden, Germany, 2005

[2] Mikalsen R, Roskilly AP. The control of a free-piston engine generator. Part 2: Engine dynamics and piston motion control. Appl Energy (2009), doi: 10.1016/ j.apenergy.2009.06.035

[3] Goertz M, Peng LX. Free piston engine its application and optimization. SAE paper 2000-01-0996, 2000

[4] Atkinson C, Petreanu S, Clark NN, Atkinson RJ etc. Numerical simulation of a two-stroke engine-alternator combination. SAE Technical Paper 1999-01-0921, 1999
[5] Shoukry E, Taylor S, Clark N. Numerical simulation for parametric study of a two-stroke direct injection linear engine. SAE paper 2002-01-1739, 2002
[6] Max E. FPEC, Free piston energy converter. In Proceedings of the 21st Electric Vehicle Symposium & Exhibition, EVS21, Monaco, 2005
[7] Blarigan PV, Paradiso N, Goldsborough SS. Homogeneous charge compression ignition with a free piston: A new approach to ideal Otto cycle performance. SAE paper 982484, 1998
[8] Blarigan PV. Advanced internal combustion electrical generator. Proceedings of the 2002 U.S. hydrogen program review, NREL/CP-610-32405, 2002
[9] Fredrisksson J, Denbratt I. Simulation of a two-stroke free piston engine. SAE paper 2004-01-1871, 2004
[10] Nemecek P, Vysoky O. Control of two-stroke free-piston generator. Proceeding of the 6th Asian control conference, 2006
[11] Mikalsen R, Roskilly AP. The design and simulation of a two-stroke free piston engine for electric power generation. Appl. Therm. Eng. (2007), doi: 10.1061/j.applthermaleng. 2007.04.009
[12] Mikalsen R, Roskilly AP. A computational study of free-piston diesel engine combustion, Appl Energ (2008), doi: 10.1016/j.apenergy.2008.08.004
[13] Xiao J et al. Motion characteristic of a free piston linear engine. Appl Energy (2009), doi:10.1016/j.apenergy.2009.07.005
[14] Cawthorne WR, Famouri P, Chen JD. Development of a linear alternator-engine for hybrid electric vehicle application. IEEE transactions on vehicular technology, vol.48, NO.6, 1999
[15] Wang JB, Howe H. A linear permanent magnet generator for a free-piston energy converter. 2005 IEEE International Conference on Electric Machines and Drives, p1521-1528, 2005
[16] Deng Z, Bold I, Nasar SA. Fields in permanent magnet linear synchronous machines. IEEE Transactions on magnets. Vol. MAG-22, NO.2, 1986
[17] Němeček P, Vysoký O. Modeling and control of free-piston generator. IFAC Mechatronic systems, Sydney, Australia, 2004
[18] Caresana F, Comodi G, Pelagalli L. Design approach for a two-stroke free piston engine for electric power generation. Society of Automotive Engineers of Japan 2004-32-0037, 2004
[19] Hohenberg GF. Advanced approaches for heat transfer calculations. SAE Special Publications. SP-449, pp. 61-79, 1979
[20] Stone R. Introduction to internal combustion engine. ISBN 0-7680-0495-0, Society of Automotive Engineers, Inc. Warrendale, Pa, 1999
[21] Nagy CT. Linear engine development for series hybrid electrical vehicles. Dissertation, West Virginia: West Virginia University, 2004
[22] Buckingham, Edgar (1914). On Physically Similar Systems: Illustrations of the Use of Dimensional Analysis. Phys. Rev. 4: 345. doi:10.1103/PhysRev.4.345
[23] Goldsborough SS, Blarigan PV. A numerical study of a free piston IC engine operating on homogeneous charge compression ignition combustion. SAE paper 990619, 1999
[24] Goldsborough SS, Blarigan PV. Optimizing the scavenging system for a two-stroke cycle, free piston engine for high efficiency and low emissions: A computational approach. International Multidimensional Engine Modeling User's Group Meeting at the SAE Congress 2003, 2003
[25] Bergman M, Fredriksson J, Golovitchev VI. CFD-Base Optimization of a Diesel-fueled Free Piston Engine Prototype for Conventional and HCCI Combustion. SAE 2008-01-2423, 2008

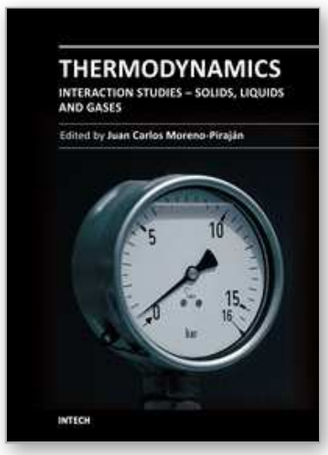


**Thermodynamics - Interaction Studies - Solids, Liquids and Gases**
Edited by Dr. Juan Carlos Moreno PirajÃ¡n

ISBN 978-953-307-563-1
Hard cover, 918 pages
**Publisher** InTech
**Published online** 02, November, 2011
**Published in print edition** November, 2011

Thermodynamics is one of the most exciting branches of physical chemistry which has greatly contributed to the modern science. Being concentrated on a wide range of applications of thermodynamics, this book gathers a series of contributions by the finest scientists in the world, gathered in an orderly manner. It can be used in post-graduate courses for students and as a reference book, as it is written in a language pleasing to the reader. It can also serve as a reference material for researchers to whom the thermodynamics is one of the area of interest.

**How to reference**
In order to correctly reference this scholarly work, feel free to copy and paste the following:

Jinlong Mao, Zhengxing Zuo and Huihua Feng (2011). Dimensionless Parametric Analysis of Spark Ignited Free-Piston Linear Alternator, Thermodynamics - Interaction Studies - Solids, Liquids and Gases, Dr. Juan Carlos Moreno PirajÃ¡n (Ed.), ISBN: 978-953-307-563-1, InTech, Available from: http://www.intechopen.com/books/thermodynamics-interaction-studies-solids-liquids-and-gases/dimensionless-parametric-analysis-of-spark-ignited-free-piston-linear-alternator

INTECH
open science | open minds

**InTech Europe**
University Campus STeP Ri
Slavka Krautzeka 83/A
51000 Rijeka, Croatia
Phone: +385 (51) 770 447
Fax: +385 (51) 686 166
www.intechopen.com

**InTech China**
Unit 405, Office Block, Hotel Equatorial Shanghai
No.65, Yan An Road (West), Shanghai, 200040, China
中国上海市延安西路65号上海国际贵都大饭店办公楼405单元
Phone: +86-21-62489820
Fax: +86-21-62489821

IntechOpen